J|A|C|S
ARTICLES
Published on Web 01/05/2007

Molecular and Electronic Structures of the Long-Bonded π-Dimers of Tetrathiafulvalene Cation-Radical in Intermolecular Electron Transfer and in (Solid-State) Conductivity

Sergiy V. Rosokha and Jay K. Kochi*

Contribution from the Department of Chemistry, University of Houston, Houston, Texas 77204

Received June 13, 2006; E-mail: jkochi@uh.edu

Abstract: Tetrathiafulvalene (**TTF**) as the prototypical electron donor for solid-state (electronics) applications is converted to the unusual cation-radical salt, $\mathbf{TTF}^{+\bullet}$ CB^- (where CB^- is the non-coordinating *closo*-dodecamethylcarboranate), for crystallographic and spectral analyses. Near-IR studies establish the spontaneous *self-association* of $\mathbf{TTF}^{+\bullet}$ to form the diamagnetic [$\mathbf{TTF}^+$,$\mathbf{TTF}^+$] dication and to also undergo the equally rapid *cross-association* with its parent donor to form the mixed-valence [$\mathbf{TTF}^{+\bullet}$,**TTF**] cation-radical. The latter, most importantly, represents the first (dyad) member of a series of p-doped tetrathiafulvalene (stacked) arrays, and the thorough scrutiny of its electronic structure with the aid of Mulliken−Hush (two-state) analysis of the diagnostic (intervalence) NIR band reveals Robin−Day Class II behavior. The theoretical consequences of the unique structure of the mixed-valence [$\mathbf{TTF}^{+\bullet}$,**TTF**] dyad on (a) the electron-transfer mechanism for self-exchange, (b) the molecular-orbital analysis of the Marcus reorganization energy, and (c) the ab initio computation of the coupling element or transfer integral in p-doped (solid-state) arrays are discussed.

Introduction

In molecule-based electronics, especially for the development of organic semiconductors and superconductors, the tetrathiafulvalene heterocycle (**TTF**) and its congeners are among the most widely utilized components,[1,2] owing to their highly desirable (donor) properties for such solid-state applications. Consequently, in p-doped tetrathiafulvalene stacks, all intermolecular interactions of the cation-radical moiety ($\mathbf{TTF}^{+\bullet}$) with its crystalline neighbors play central and pivotal roles in limiting the electronics efficacy.[2,3]

According to the conventional solid-state (tight-binding) model,[2−4] the strong electronic coupling extant between the cation-radical and neutral parent (i.e., the $\mathbf{TTF}^{+\bullet}$/**TTF** dyad associate) leads to π-electron delocalization, and the mobility of the charge carrier within the array is related to the conduction bandwidth, given as 4 times the coupling matrix element V (also referred to as the transfer integral and otherwise designated as H_{ab}, β, or t[2−5]). However, any strong π-bonding between a pair of $\mathbf{TTF}^{+\bullet}$ neighbors can lead to diamagnetic dimers and thus result in nonconducting (insulator) states.

At the other limit of weak electronic coupling, the charge mobility is determined by the electron hopping between the charged $\mathbf{TTF}^{+\bullet}$ and neutral **TTF** moieties with a rate constant that is commonly taken to be exponentially dependent on the V-adjusted barrier, i.e., $(\lambda - 2V)^2/4\lambda$, where λ is the Marcus reorganization energy,[6,7] and the pre-exponential factor is proportional to the square of the coupling element for $V \lesssim 10$ cm^{-1}, representative of non-adiabatic electron transfers.[8] [Note that, for strong coupling diagnostic of adiabatic electron transfer, the pre-exponential constant is merely equated to the calculated frequency of the nuclear motion along the reaction coordinate.[8]] As the result of these theoretical insights, there has been a flurry of recent interest in the quantitative assessment of the basic parameters (V and λ) for electron transfer and π-delocalization,[3−6,9] especially as they apply to various solid-state tetrathiafulvalene arrays.[10]

(1) (a) *TTF Chemistry: Fundamentals and Applications of Tetrathiafulvalene*; Yamada, J.-I., Sugimoto, T., Eds.; Kodansha Springer: Berlin, 2004. (b) Khodorkovsky, V.; Becker, J. Y. In *Organic Conductors: Fundamentals and Applications*; Farges, J.-P., Ed.; Marcel Dekker: New York, 1994. (c) Bendikov, M.; Wudl, F.; Perepichka, D. F. *Chem. Rev.* **2004**, *104*, 4891.
(2) (a) Williams, J. M. *Organic Superconductors: Synthesis, Structure, Properties and Theory*; Prentice Hall: Englewood Cliffs, NJ, 1992. (b) Miller, J. S., Drillon, M., Eds. *Magnetism: Molecules to Materials*; Wiley-VCH: Weinheim, 2001. (c) Ferraro, J. R.; Williams, J. M. *Introduction to Synthetic Electrical Conductors*; Academic: Orlando, FL, 1987. (d) Miller, J. S., Ed. *Extended Linear Chain Compounds*, Vols. 2 and 3; Plenum Press: New York, 1983. (e) Soos, Z. G.; Klein, D. J. In *Molecular Association*, Vol. 1; Foster, R., Ed.; Academic: New York, 1975. (f) See also: Batail, P. Guest Ed., Molecular Conductors Thematic Issue. *Chem. Rev.* **2004**, *104* (11).
(3) (a) Haddon, R. C.; Siegriest, T.; Fleming, R. M.; Bridenbaugh, P. M.; Laudise, R. A. *J. Mater. Chem.* **1995**, *5*, 1719. (b) Bromley, S. T.; Mas-Torrent, M.; Hadley, P.; Rovgira, C. *J. Am. Chem. Soc.* **2004**, *126*, 6544.
(4) Bredas, J. L.; Calbert, J. P.; da Silva Filho, D. A.; Cornil, J. *Proc. Natl. Acad. Sci. U.S.A.* **2002**, *99*, 5804.
(5) (a) Hutchison, G. R.; Ratner, M. A.; Marks, T. J. *J. Am. Chem. Soc.* **2005**, *127*, 2339. (b) Hutchison, G. R.; Ratner, M. A.; Marks, T. J. *J. Am. Chem. Soc.* **2005**, *127*, 16881.
(6) Kwon, O.; Coropceanu, V.; Gruhn, N. E.; Durivage, J. C.; Laquindanum, J. G.; Katz, H. E.; Cornil, J.; Bredas, J. L. *J. Chem. Phys.* **2004**, *120*, 8186.
(7) (a) Marcus, R. A. *Rev. Mod. Phys.* **1993**, *65*, 599. (b) Sutin, N. *Prog. Inorg. Chem.* **1983**, *30*, 441.
(8) (a) Brunschwig, B. S.; Sutin, N. *Coord. Chem. Revs.* **1999**, *187*, 233. (b) Brunschwig, B. S.; Sutin, N. In *Electron Transfer in Chemistry*; Balzani, V., Ed.; Wiley: New-York, 2001, Vol. 2, p 583.

10.1021/ja064166x CCC: $37.00

It is important to emphasize, however, that in the solid state the critical parameters for the electronic coupling element (V) and the reorganization energy (λ) relate to crystalline properties and are experimentally difficult to evaluate unambiguously due to the "infinite" nature of the π-stacking in **TTF** arrays. Consequently, theoretical treatments of electron π-delocalization and hopping have by and large depended on models based on pairwise orbital splittings.[9−11] Accordingly, it is now opportune to unequivocally establish the thermodynamics framework for the quantitative assessment of the coupling element and reorganization energy that can only be experimentally obtained following the diffusive encounter of $\mathbf{TTF}^{+\bullet}$ with its pertinent solid-state neighbor in *solution.* Thus, we believe the binary (intermolecular) interaction of $\mathbf{TTF}^{+\bullet}$ with the parent **TTF** donor will yield unambiguous values of these important parameters and, it is hoped, shed light on the assessment of π-delocalization in conducting solids. Likewise, the thermodynamics of the self-association of $\mathbf{TTF}^{+\bullet}$ in solution will lead to the assessment of the π-dimerization pertinent to nonconducting states. Indeed, independent methodologies are available for the quantitative evaluations of both electron-transfer parameters for discrete mixed-valence or donor/acceptor dyads from their spectral characteristics, as developed by Hush[12] on the basis of Mulliken charge-transfer theory.[13] According to the Mulliken−Hush formulation of localized π-complexes with weak coupling, the reorganization energy for thermal electron transfer in solution is directly related to the energy of the optical (intervalence) transition, i.e., $\lambda = \nu_{IV}$. In such mixed-valence complexes, the electronic coupling element is designated as H_{ab} (to distinguish it from the corresponding solid-state parameter V), and its magnitude is related to the intensity of the intervalence absorption:

$$H_{ab} = 0.0206(\nu_{IV}\,\Delta\nu_{1/2}\,\epsilon_{IV})^{1/2}/r_{DA} \qquad (1)$$

where ν_{IV} and $\Delta\nu_{1/2}$ are the spectral maximum and full width at half-maximum (cm^{-1}) of the intervalence band, ϵ_{IV} is its extinction coefficient ($M^{-1}\,cm^{-1}$), and r_{DA} is the separation (Å) between the (donor/acceptor) redox centers. On the other hand, in delocalized complexes with $\lambda < 2H_{ab}$, the coupling element is equal to the energy of the optical transition between the donor (HOMO) and the acceptor (LUMO) centers, i.e., $\nu_{IV} = 2H_{ab}$.[8,14] The Hush methodology has been successfully used for the experimental determination of the kinetic parameters governing thermal electron transfer in a variety of bridged mixed-valence systems,[15] and our recent studies[16,17] demonstrate that it is also applicable to intermolecular (face-to-face) π-donor/acceptor associates earlier described as Mulliken charge-transfer (CT) complexes.[18] Such π-complexes between organic ion-radicals and their parent π-donors represent the transient precursors to intermolecular ET self-exchange, as described for the cation-radical $\mathbf{D}^{+\bullet}$ in eq 2:

$$\mathbf{D} + \mathbf{D}^{+\bullet} \overset{K_{CT}}{\rightleftharpoons} [\mathbf{D},\mathbf{D}^{+\bullet}] \overset{k_{ET}}{\rightleftharpoons} [\mathbf{D}^{+\bullet},\mathbf{D}] \rightleftharpoons \mathbf{D}^{+\bullet} + \mathbf{D} \qquad (2)$$

In earlier studies, we showed that isolation of the dimeric ion-radicals[19] from solution, together with their spectral characterization according to the Mulliken−Hush formalism, leads to the values of H_{ab} and λ which have been supported by independent quantum-mechanical calculations.[17] Moreover, the evaluation of H_{ab} and λ will allow the consistent interpretation of the fast kinetics for the ET self-exchange of organic ion-radicals according to the mechanism in eq 2.[16,17]

We provide in this study the critical evaluation of the principal electron-transfer parameters of tetrathiafulvalene for comparison with the solid-state data[20] and those obtained by theoretical computations,[10] as well as kinetic data on the $\mathbf{TTF}^{+\bullet}$/**TTF** self-exchange in solution.[21] Although definitive X-ray structural data[22,23] are available for various solid-state assemblies of **TTF** and $\mathbf{TTF}^{+\bullet}$, there is surprisingly no information relating to the intermolecular (binary) association of the cation-radical with the parent donor, i.e.,

$$\mathbf{TTF}^{+\bullet} + \mathbf{TTF} \overset{K_{CT}}{\rightleftharpoons} [\mathbf{TTF}^{+\bullet},\mathbf{TTF}] \qquad (3)$$

the charge-transfer or π-complex of which has never been

(9) (a) Gruhn, N. E.; da Silva Filho, D. A.; Bill, T. G.; Malagali, M.; Coropceanu, V.; Kahn, A.; Bredas, J. L. *J. Am. Chem. Soc.* **2002**, *124*, 7918. (b) Senthilkumar, K.; Grozema, F. C.; Bickelhaupt, F. M.; Siebbeles, L. D. A. *J. Chem. Phys.* **2003**, *119*, 9809. (c) Koren, A. B.; Curtis, M. D.; Francis, A. H.; Kampf, J. W. *J. Am. Chem. Soc.* **2003**, *125*, 5040. (d) Huang, J.; Kertesz, M. *J. Phys. Chem. B* **2005**, *109*, 12891. (e) Troisi, A.; Orlandi, G. *J. Phys. Chem. A* **2006**, *110*, 4065.

(10) (a) Huang, J.-S.; Kertesz, M. *Chem. Phys. Lett.* **2004**, *390*, 110. (b) Huang, J.-S.; Kertesz, M. *J. Chem. Phys.* **2005**, *122*, 234707.

(11) Newton, M. D. *Chem. Rev.* **1991**, *91*, 767.

(12) Hush, N. S. *Prog. Inorg. Chem.* **1967**, *8*, 391.

(13) Mulliken, R. S.; Person, W. B. *Molecular Complexes*; Wiley: New York, 1969.

(14) However, for a recent discussion of the validity of this relationship based on the study of somewhat related *bridged* mixed-valence systems, see: Nelsen, S. F.; Luo, Y.; Weaver, M. N.; Lockard, J. V.; Zink, J. F. *J. Org. Chem.* **2006**, *71*, 4286.

(15) (a) Creutz, C. *Prog. Inorg. Chem.* **1983**, *30*, 1. (b) Elliot, C. M.; Derr, D. L.; Matyushov, D. V.; Newton, M. D. *J. Am. Chem. Soc.* **1998**, *120*, 11714. (c) Lahlil, K.; Moradpour, A.; Bowlas, C.; Menou, F.; Cassoux, P.; Bonvoisin, J.; Launay, J.-P.; Dive, G.; Dehareng, D. *J. Am. Chem. Soc.* **1995**, *117*, 9995. (d) Nelsen, S. F.; Ismagilov, R. F.; Powell, D. R. *J. Am. Chem. Soc.* **1997**, *119*, 10213. (e) Lambert, C.; Noll, G. *J. Am. Chem. Soc.* **1999**, *121*, 8434. (f) Lindeman, S. V.; Rosokha, S. V.; Sun, D.-L.; Kochi, J. K. *J. Am. Chem. Soc* **2002**, *124*, 843.

(16) (a) Ganesan, V.; Rosokha, S. V.; Kochi, J. K. *J. Am. Chem. Soc.* **2003**, *125*, 2559. (b) Sun, D.; Rosokha, S. V.; Lindeman, S. V.; Kochi, J. K. *J. Am. Chem. Soc.* **2003**, *125*, 15950. (c) Sun, D.; Rosokha, S. V.; Kochi, J. K. *J. Am. Chem. Soc.* **2004**, *126*, 1388.

(17) (a) Rosokha, S. V.; Lu, J.-M.; Newton, M. D.; Kochi, J. K. *J. Am. Chem. Soc.* **2005**, *127*, 7411. (b) Rosokha, S. V.; Newton, M. D.; Head-Gordon, M.; Kochi, J. K. *Chem. Phys.* **2006**, *324*, 117.

(18) (a) Kochi, J. K.; Rathore, R.; Le Magueres, P. *J. Org. Chem.* **2000**, *65*, 6826. (b) LeMagueres, P.; Lindeman, S. V.; Kochi, J. K. *Org. Lett.* **2000**, *2*, 3562.

(19) (a) For electron-transfer (self-exchange) studies of organic donor/acceptor redox pairs, equivalent (phenomenological) kinetics are obtained for the donor (D) and its cation-radical ($D^{+\bullet}$), as well as the acceptor (A) and its anion radical ($A^{-\bullet}$), in which the mixed-valence dyads represent p-doping and n-doping, respectively, of stacked arrays. (b) As employed here, the dimeric ion radicals or Hush intervalence (IV) dyads[12] are equivalent to traditional Mulliken charge-transfer (CT) complexes.[13,14a,18] Therefore, to maintain historical integrity, the notations CT and IV are hereinafter referred to interchangeably.

(20) (a) Heger, A. J. In *Highly Conducting One-Dimensional Solids*; Devreese, J. T., Evrard, R. P., van Doren, V. E., Eds.; Plenum Press: New York, 1979; p 69. (b) S. Shitzkovsky, S.; Weger, M.; Gutfreund, H. *J. Phys. (Paris)* **1978**, *39*, 711.

(21) (a) Grampp, G.; Jaenicke, W. *Ber. Bunsenges. Phys. Chem.* **1991**, *95*, 904. (b) Grampp, G.; Kapturkiewicz, A.; Jaenicke, W. *Ber. Bunsenges. Phys. Chem.* **1991**, *94*, 439.

(22) (a) Yakushi, K.; Nishimura, S.; Sugano, T.; Kuroda, H. *Acta Crystallogr. B* **1980**, *36*, 358. (b) Kondo, K.; Matsubayashi, G.; Tanaka, T.; Yoshioka, H.; Nakatsu, K. *J. Chem. Soc., Dalton Trans.* **1984**, 379. (c) Legros, J.-P.; Bousseau, M.; Valade, L.; Cassoux, P. *Mol. Cryst. Liq. Cryst.* **1983**, *100*, 181. (d) Umeya, M.; Kawata, S.; Matsuzaka, H.; Kitagawa, S.; Nishikawa, H.; Kikuchi, K.; Ikemoto, I. *J. Mater. Chem.* **1998**, *8*, 295. (e) Ouahab, L.; Fettouhi, M.; Halet, J. F.; Yartsev, V. M.; Garrigou-Lagrange, C.; Delhaes, P.; Sourisseau, C. *New J. Chem.* **1993**, *17*, 399. (f) Ouahab, L.; Padiou, J.; Grandjean, D.; Garrigou-Lagrange, C.; Delhaes, P.; Bencharif, M. *J. Chem. Soc., Chem. Commun.* **1989**, 1038. (g) Pyrka, G. J.; Fernando, Q.; Inoue, M. B.; Inoue, M. *Inorg. Chim. Acta* **1989**, *156*, 257. (h) Kathirgamanathan, P.; Mazid, M. A.; Rosseinsky, D. R. *J. Chem. Soc., Perkin Trans. 2* **1982**, 593.

(23) (a) Blessing, R. H.; Coppens, P. *Solid State Commun.* **1974**, *15*, 215. (b) Kistenmacher, T. J.; Phillips, T. E.; Cowan, D. O. *Acta Crystallogr. B* **1974**, *30*, 763.

detected in solution. By way of comparison, the analogous π-association of a pair of cation-radicals resulting in the diamagnetic dicationic dimer, i.e.,

$$\mathbf{TTF}^{+\bullet} + \mathbf{TTF}^{+\bullet} \overset{K_D}{\rightleftharpoons} [\mathbf{TTF}^{+\bullet},\mathbf{TTF}^{+\bullet}] \qquad (4)$$

has been observed by UV−vis and ESR spectroscopy at very low temperatures in ethanol,[24,25] but no thermodynamic data are available for cation-radical dimerization.

The π-dimerizations of the tetrathiafulvalene cation-radical, as described in eqs 3 and 4, are of paramount importance for conductor/insulator modeling of p-doped solid-state arrays. However, despite a number of attempts, no exhaustive data for the existence of such intermolecular dimerizations have been forthcoming, although as an "artificial" alternative, several authors have recently resorted to indirect methods for enforced (dyad) interactions, such as in (a) the synthesis of intramolecular (mixed-valence) models of the general structure **TTF**$^{+\bullet}$−bridge−**TTF**[26a−c] or (b) the forced juxtaposition of **TTF**$^{+\bullet}$/**TTF** dyads via intercalation into a self-assembled molecular "cage".[26d] Accordingly, our first objective here is to establish the definitive properties of both π-dimeric species, i.e., as the dicationic [**TTF**$^{+\bullet}$,**TTF**$^{+\bullet}$] dyad and the cation-radicaloid [**TTF**$^{+\bullet}$,**TTF**] dyad, with particular regard to (1) the spectral characterization and thermodynamics measurement of the equilibria in eqs 3 and 4, (2) the common long-bonded character of the π-dimers with overall +1 and +2 charges, (3) the quantitative evaluation of the electronic coupling element H_{ab} and the reorganization energy λ governing the electron-transfer process within **TTF**$^{+\bullet}$/**TTF** dyads, (4) the validation of the H_{ab} and λ parameters for the proper description of the self-exchange processes in solution, and most importantly, (5) the establishment of the relationship of H_{ab} and λ with the corresponding parameters determined from solid-state and computational studies.

Results

Critical to our study of the π-associations of **TTF**$^{+\bullet}$ (eqs 3 and 4) was the availability of a pure salt comprised of a large non- (or very weakly) coordinating counteranion to minimize ion-pairing effects in a weakly polar solvent such as dichloromethane and thus allow the comparison of the solution data with those resulting from solid-state and computational (in vacuo) studies.

1. Preparation and Structural Characterization of the Soluble TTF$^{+\bullet}$ Salt. The excellent electron-donor properties of tetrathiafulvalene, with its reversible oxidation potential of $E_{ox}° = 0.37$ V vs SCE,[1a] enables the ready and quantitative one-electron oxidation with stoichiometric amounts of permethylcarboranyl (CB$^{\bullet}$), with $E_{red} = 1.4$ V[16c,27,28] in dichloromethane solution, according to the 1:1 stoichiometry in eq 5: The pure paramagnetic salt **TTF**$^{+\bullet}$CB$^-$ was easily separated in

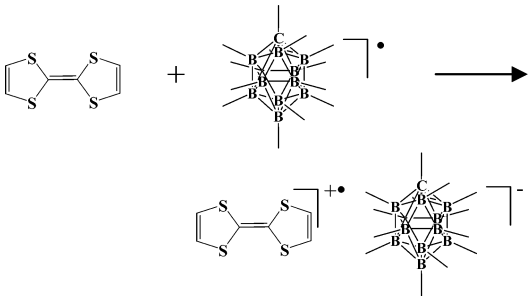

(5)

nearly quantitative yield simply by the addition of hexane, and the purity of the almost black microcrystals was found by spectral titration to be >98% (see Experimental Section).

The X-ray crystallographic analysis of the dark brown single crystal obtained by slow diffusion of hexane into a solution of **TTF**$^{+\bullet}$CB$^-$ in dichloromethane (Figure 1) demonstrates the cation/anion interchanges to occur freely in the crystal lattice in both horizontal and vertical directions. The essentially planar **TTF**$^{+\bullet}$ moiety is centrosymmetric and shows an elongated central double bond of 1.397 Å and significantly shortened C−S bonds of 1.717 Å, as compared to the corresponding values of 1.350 and 1.760 Å, respectively, in the neutral donor.[29]

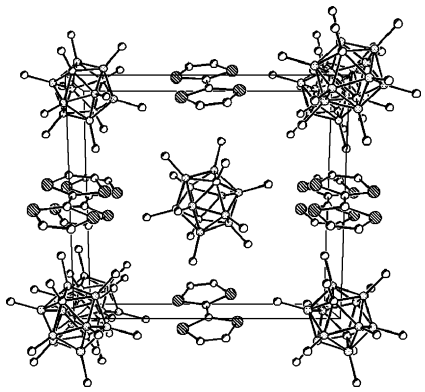

Figure 1. Unit cell of the (**TTF**$^{+\bullet}$CB$^-$) salt, showing limited (well-separated) ion-pair interactions resulting from relatively simple cation/anion interchanges.

Most importantly, the absence of any close cation/anion or cation/cation contacts in the unit cell, together with the extensive charge delocalization within CB$^-$ and the absence of external distortion in **TTF**$^{+\bullet}$, indicates that all interionic (electrostatic) interactions are minimal. We thus conclude that **TTF**$^{+\bullet}$ in this 1:1 salt is very close to being a "free" cationic species in the solid state as well as in solution.[30]

2. π-Dimerization of Tetrathiafulvalene Cation-Radicals. 2.1. Spectral (UV−Vis) Observation of the Self-Association

(24) Torrance, J. B.; Scott, B. A.; Welber, B.; Kaufman, F. B.; Seiden, P. E. *Phys. Rev. B* **1979**, *19*, 730.
(25) Khodorkovsky, V.; Shapiro, L.; Krief, P.; Shames, A.; Mabon, G.; Gorgues, A.; Giffard, M. *Chem. Commun.* **2001**, 2736.
(26) (a) Spanggaard, H.; Prehn, J.; Nielsen, M. B.; Levillain, E.; Allain, M.; Becher, J. *J. Am. Chem. Soc.* **2000**, *122*, 9486. (b) Iyoda, M.; Hasegawa, M.; Kuwatani, Y.; Nishikawa, H.; Fukami, K.; Nagase, S.; Yamamoto, G. *Chem. Lett.* **2001**, 1146. (c) Lyskawa, J.; Salle, M.; Balandier, J.-Y.; Le Derf, F.; Levillain, E.; Allain, M.; Viel, P.; Palacin, S. *Chem. Commun.* **2006**, 2233. (d) Yoshizawa, M.; Kumazawa, K.; Fujita, M. *J. Am. Chem. Soc.* **2005**, *127*, 13456.
(27) For the preparation and characterization of CB$^{\bullet}$, see: King, B. T.; Noll, B. C.; McKinley, A. J.; Michl, J. *J. Am. Chem. Soc.* **1996**, *118*, 10902.
(28) (a) Sun, D.; Rosokha, S. V.; Kochi, J. K. *Angew. Chem.* **2005**, *44*, 5133. (b) Rosokha, S. V.; Neretin, I. S.; Sun, D.; Kochi, J. K. *J. Am. Chem. Soc.* **2006**, *127*, 9394.
(29) (a) Cooper, W. F.; Edmonds, J. W.; Wudl, F.; Coppens, P. *′ Cryst. Struct. Commun.* **1974**, *3*, 23. (b) The C−S and C−C bond lengths determined in the +1 cation-radical are close to the average values for the corresponding bond lengths taken over an extended set of salts with different counterions.[29c−e] For other systems with partial charge-transfer, see: (c) Umland, T. C.; Allie, S.; Kuhlmann, T.; Coppens, P. *J. Phys. Chem.* **1988**, *92*, 6456. (d) Clemente, D. A.; Marzotto, A. *J. Mater. Chem.* **1996**, *6*, 941. (e) Le Cointe, M.; Lemee-Cailleau, M. H.; Cailleau, H.; Toudic, B.; Toupet, L.; Heger, G.; Moussa, F.; Schweiss, P.; Kraft, K. H.; Karl, N. *Phys. Rev. B* **1995**, *51*, 3374. (f) Rosokha, S. V.; Dibrov, S. M.; Rosokha, T. Y.; Kochi, J. K. *Photochem. Photobiol. Sci.* **2006**, *5*, 914.
(30) Lu, J. M.; Rosokha, S. V.; Lindeman, S. V.; Neretin, I. S.; Kochi, J. K. *J. Am. Chem. Soc.* **2005**, *127*, 1797.

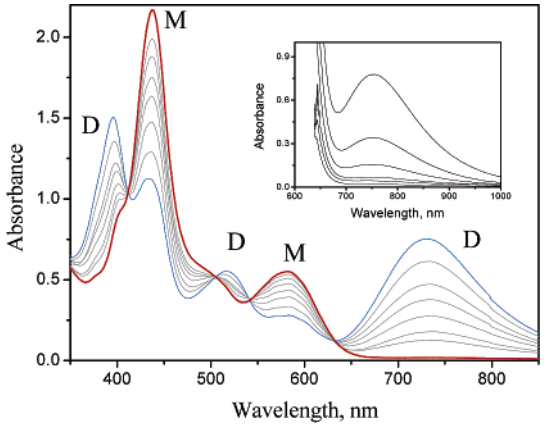

Figure 2. Temperature-dependent absorption of 1.3 mM solutions of **TTF**$^{+\bullet}$**CB**$^-$ in acetone, showing reversible interconversion between the electronic spectrum of the monomer M (prevailing at room temperature) and the dimer D (at low temperature). Temperature (in °C, from bottom to top at 740 nm): 22, −40, −55, −63, −70, −78, −85, and −90. Inset: Low-energy range of the absorption at high concentrations of **TTF**$^{+\bullet}$**CB**$^-$ (λ = 2 mm, 22 °C). Concentration of **TTF**$^{+\bullet}$**CB**$^-$ (in mM, bottom to top): 0, 4.7, 6.2, 9.3, 13, and 19.

of TTF$^{+\bullet}$**.** The electronic (UV−vis) spectrum in Figure 2 (red curve) of **TTF**$^{+\bullet}$**CB**$^-$ dissolved in acetone consisted of a major band at λ_M = 438 nm ($\epsilon = 1.6 \times 10^4$ M^{-1} cm^{-1}) and a minor one at 582 nm ($\epsilon = 4.2 \times 10^3$ M^{-1} cm^{-1}), and these both agreed with previous reports (in other solvents) and were confirmed by theoretical calculations.[25,31a]The absorbance increase of the twin absorption bands was linear at low concentrations of 0.1−1.0 mM, expected for **TTF**$^{+\bullet}$ as the monomeric species. However, in more concentrated (>5 mM) solutions, a new broad (low-energy) band appeared at λ_D = 752 nm (Figure 2 and Figure S1 in the Supporting Information), and its absorbance increase showed a quadratic concentration dependence (see Experimental Section and Table S1 and Figure S2 in the Supporting Information), symptomatic of the dimeric species, (**TTF**$^{+\bullet}$)$_2$. Indeed, the latter progressively grew as the solution was gradually cooled from room temperature to < −100 °C, as shown by the incremental increase of the low-energy absorbance in the 650−850-nm range (Figure 2).[31b] The temperature-dependent reversible dimerization of **TTF**$^{+\bullet}$ according to eq 4 was confirmed by the concomitant decrease in the concentration of monomeric **TTF**$^{+\bullet}$, as indicated by the attenuation of the 438/582-nm bands as these were successively replaced by the corresponding UV bands of dimeric (**TTF**$^{+\bullet}$)$_2$, with λ_D = 395/520 nm, and showing four clearly resolved isosbestic points at 413, 502, 543, and 631 nm (Figure 2). Most importantly at our lowest measurable temperatures, the absorption spectrum shown as the blue curve in Figure 2 was quite similar to the spectral characteristics of the solid-state absorption spectrum of tetrathiafulvalene dimer first reported by Torrance and co-workers.[24]

2.2. ESR Measurements of the Reversible Dimerization of TTF$^{+\bullet}$**.** Further support for the concentration- and temperature-dependent dimerization of **TTF**$^{+\bullet}$ was provided by the accompanying changes in the ESR spectrum of the monomeric salt **TTF**$^{+\bullet}$**CB**$^-$ dissolved in acetone and showing the well-resolved binomial quintet arising from the hyperfine splitting by 4 equiv of hydrogen, with a_H = 1.26 G.[25] The gradual attenuation of this ESR spectrum as the temperature was incrementally lowered coincided with the replacement of monomeric **TTF**$^{+\bullet}$ with the ESR-silent (diamagnetic) dimer.[25,32] The fraction (α_M) of monomeric **TTF**$^{+\bullet}$ was evaluated directly by double integration of the series of temperature-dependent ESR spectra, and the unmistakable fit of the calculated concentration change according to eq 4 is illustrated in Figure 3. Figure 3 also includes the corresponding changes in α_M, as evaluated from the temperature-dependent variation of the visible absorbance at λ_D = 752 nm.[31b] Their concordance within the accuracy limits of the ESR measurements thus validates the presence of the monomer−dimer equilibrium of **TTF**$^{+\bullet}$ according to eq 4. These spectral fits allowed the dimerization constant of K_D = 0.6 M^{-1} to be evaluated at 295 K, and the linear dependence of log K_D with inverse temperature afforded the thermodynamic parameters ΔH_D = −8 kcal M^{-1} and ΔS_D = −28 eu.

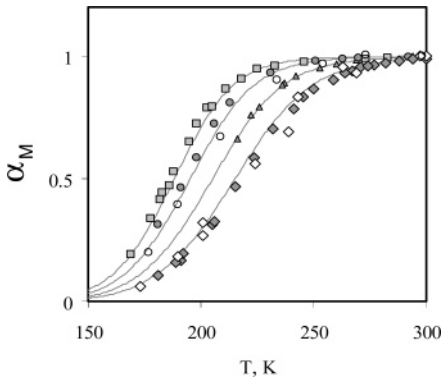

Figure 3. Temperature dependence of the monomer fraction (α_M) calculated from the absorption (filled symbols) and ESR (open symbols) measurements of **TTF**$^{+\bullet}$**CB**$^-$ in acetone. Concentration of **TTF**$^{+\bullet}$**CB**$^-$ (in mM): 0.7 (squares), 2 (circles), 4 (triangles), and 10 (rombics). The gray lines represent the values of α_M calculated for the monomer/dimer equilibrium with ΔH = −8.0 kcal/mol and ΔS = −28 eu.

2.3. Solvent Effects on the Thermodynamics of TTF$^{+\bullet}$ **Dimerization.** Solutions of **TTF**$^{+\bullet}$**CB**$^-$ in polar solvents such as ethanol (see Figures S3−S5 and Table S2), acetonitrile, and dimethylformamide (Figures S6 and S7) showed temperature- and concentration-dependent spectral changes that were more or less comparable to those in observed in acetone. However, in less polar solvents such as dichloromethane or tetrahydrofuran, the dimeric species were only observed at very low (−70 to −90 °C) temperatures and at very high concentrations of **TTF**$^{+\bullet}$**CB**$^-$ (Figure S7). As such, the high-energy absorption bands were overshadowed by the monomer absorption, and only the low-energy dimer band at $\lambda_D \approx$ 735 nm could be measured well. Finally, in toluene and diethyl ether, the limited solubility of **TTF**$^{+\bullet}$**CB**$^-$ precluded the direct observation of the diagnostic dimer bands.

Quantitative spectral measurements of solvent effects (Table 1) provided valuable thermodynamic and spectroscopic insight into the **TTF**$^{+\bullet}$ dimerization. First, spectral measurements in a particular solvent yielded only one set of thermodynamic parameters, ΔH_D and ΔS_D (within the accuracy limit), over a wide range of concentrations and temperatures; this validated the spectral assignment to a single (reversible) equilibrium

(31) (a) Pou-Amerigo, R.; Orti, E.; Merchan, M.; Rubio, M.; Viruela, P. M. *J. Phys. Chem. A* **2002**, *106*, 631. (b) In contrast to the local absorption band of **TTF**$^{+\bullet}$, the maximum of the low-energy band, λ_D, of the dimer shows consistent but slight blue shifts upon lowering the temperature, which we tentatively ascribe to the labile nature of such long-bonded dimeric species (vide supra).

(32) Compare: Lu, J.-M.; Rosokha, S. V.; Kochi, J. K. *J. Am. Chem. Soc.* **2003**, *125*, 12161.

Table 1. Spectral Characteristics of Monomer $\mathbf{TTF}^{+\bullet}$ (λ_M) and Dimer $(\mathbf{TTF}_2)^{2+}$ (λ_D), and Thermodynamics of Dimerization (ΔH_D, ΔS) Measured in Solution of $\mathbf{TTF}^{+\bullet}CB^-$

solvent	λ_M, nm[a]	λ_D, nm[b]	$-\Delta H_D$,[d] kcal M^{-1}	$-\Delta S_D$,[e] eu
EtOH[f]	435, 581	393, 521, 731	8.6	30
acetone	437, 581	395, 520, 730	8.0	28
DMF	442, 586	393, 515, 745[g]	7.8	26
CH_3CN	436, 581	733[c,h]	9.1	31
THF	440, 585	738[c]	5.5	22
CH_2Cl_2	440, 579	734[c]	3.8	18

[a] Extinction coefficients are 1.6×10^4 M^{-1} cm^{-1} (438 nm) and 4.2×10^3 M^{-1} cm^{-1} (582 nm) in all solvents. [b] Measured at −90 °C, unless noted otherwise. At 22 °C, low-energy maxima λ_D are 755, 752, 759, and 743 nm in EtOH, acetone, DMF, and CH_3CN, respectively; extinction coefficients are 3.0×10^4 (band at ∼390 nm), 1.2×10^4 (∼520 nm), and 2.2×10^4 M^{-1} cm^{-1} (∼730 nm). [c] High-energy bands are overshadowed by the monomer absorption. [d] ±0.5 kcal M^{-1}. [e] ±3 eu. [f] With $\mathbf{TTF}^{+\bullet}ClO_4^-$, $\Delta H = -9.5 \pm 1.0$ kcal M^{-1} and $\Delta S = 34 \pm 5$ eu. [g] At −60 °C [h] At −40 °C.

between $\mathbf{TTF}^{+\bullet}$ monomer and dimer. Second, a unique set of spectroscopic parameters was applicable to all species, irrespective of the solvent. In particular, the extinction coefficients for λ_M of $\epsilon = 1.6 \times 10^4$ and 0.42×10^4 M^{-1} cm^{-1} for the 438- and 582-nm bands, respectively, as well as those for the λ_D of $\epsilon = 3.0 \times 10^4$, 1.2×10^4, and 2.2×10^4 M^{-1} cm^{-1} for the ∼390-, ∼520-, and ∼740-nm bands, respectively, were all essentially invariant in such diverse solvents as acetonitrile, ethanol, and dichloromethane.

The results in Table 1 indicated that the enthalpy of dimer formation was more negative in polar solvents, to accord with the more favorable solvation energy of dicationic species.[33a] Furthermore, direct spectral comparisons showed that the CB^- salt of $\mathbf{TTF}^{+\bullet}$ was the same as the ClO_4^- salt, in harmony with the outer-sphere character of both pairs of salts in acetone as in ethanol.[33b,c]

3. Reversible Donor/Acceptor Association of TTF and Its Cation-Radical. 3.1. Spectral (UV−Vis) Observation and Solvent Effects on the Cross-Association of $\mathbf{TTF}^{+\bullet}$. Although separate solutions of the **TTF** donor and the cationic $\mathbf{TTF}^{+\bullet}$ were bereft of any electronic transitions in the 1000−3000-nm range, even at high concentrations and very low temperatures, various mixtures of **TTF** and $\mathbf{TTF}^{+\bullet}CB^-$ consistently showed a pronounced new broad absorption band (Figure 4) at $\lambda_{CT} =$ 2100 nm ($\epsilon = 5 \times 10^3$ M^{-1} cm^{-1}). This distinctive near-IR band[26,34] also resulted immediately upon the addition of **TTF** to a dichloromethane solution of $\mathbf{TTF}^{+\bullet}CB^-$, and it increased in intensity with the gradual lowering of the temperature (Figure S8 in the Supporting Information).

Quantitative analysis of the dependence of the absorption intensity on the concentrations of both **TTF** and $\mathbf{TTF}^{+\bullet}CB^-$ in dichloromethane (Figure 4) established the formation of the 1:1 complex according to eq 3. The equilibrium constant for the formation of this donor/acceptor complex of $K_{CT} = 6.0$ M^{-1} and its spectral characteristics derived from the concentration-dependence studies are included in Table 2; the linear dependence of ln K_{CT} on inverse temperature (inset, Figure 4) afforded the thermodynamic parameters $\Delta H_{CT} = -5.5$ kcal M^{-1} and $\Delta S_{CT} = -16$ eu.

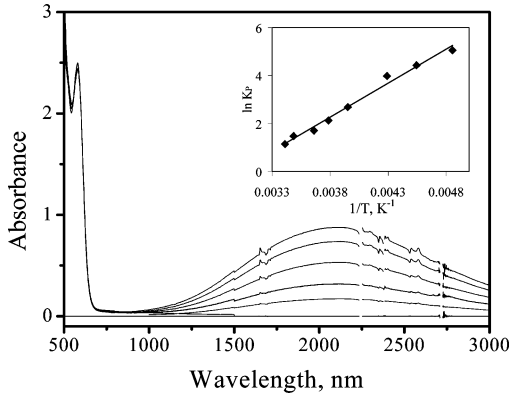

Figure 4. Spectral changes attendant upon the addition of neutral **TTF** to the 5.8 mM solution of $\mathbf{TTF}^{+\bullet}CB^-$ in CH_2Cl_2 at 22 °C. **TTF** concentration (bottom to top): 0, 44, 88, 141, 200, and 250 mM. Inset: Linear dependence of ln K_{CT} on $1/T$.

Similar NIR bands were observed upon the addition of tetrathiafulvalene to solutions of its cation-radical (or vice versa) in a variety of other solvents (Figure S9), and the analysis of the absorption intensities led to the extinction coefficients and equilibrium constants listed in Table 2. Notably, the formation of the charge-transfer or mixed-valence [$\mathbf{TTF}^{+\bullet}$,**TTF**] complex was significantly less favorable in polar solvents in contrast to the behavior of the dication dimer (vide supra). Such a dependence may be attributed to decreased solvation energy as a result of the charge delocalization spread over two **TTF** moieties.[35] Furthermore, the pronounced solvent-induced variation of the NIR band from 2115 nm in dichloromethane to about 1690 nm in DMF (Table 2) is particularly noteworthy (vide infra).

Table 2. Spectral (Charge-Transfer) Characteristics of the Mixed-Valence Dimer [$\mathbf{TTF}^{+\bullet}$,**TTF**] and Equilibrium Constant of Its Formation in Solutions of $\mathbf{TTF}^{+\bullet}CB^-$ and **TTF**

solvent	λ_{CT}, nm[a]	K_{CT}, M^{-1}	k_{SE}^{exp},[d] $\times 10^9$ M^{-1} s^{-1}
CH_2Cl_2	2115	6.0[b]	2.7 (2.9)
CH_3CN	1720	0.7[c]	3.3 (3.0)
acetone	1750	0.6	3.5 (4.0[e])
THF	1950	0.4	2.3
MeOH	1830	1.3	
DMF	1690	0.3	

[a] Extinction coefficients at λ_{IV} are $(5.0 \pm 1.0) \times 10^3$ in CH_2Cl_2 and $\sim(3.5 \pm 1.0) \times 10^3$ M^{-1} cm^{-1} in other solvents. [Note that only the product $\epsilon_{CT}K_{CT}$ was determined accurately in solvents other than CH_2Cl_2 (due to the limited formation of the mixed-valence dimer and solvent absorption interferences in the NIR range), and the accuracy of the values of ϵ and K_{CT} is ∼30%, and that for λ_{CT} is ±30 nm.] [b] $-\Delta H_{CT} = -5.5 \pm 1.0$ kcal M^{-1}; $\Delta S_{CT} = -16 \pm 3$ eu. [c] $-\Delta H_{CT} = -3.5 \pm 1.0$ kcal M^{-1}; $\Delta S_{CT} = -12 \pm 3$ eu. [d] Measured in solution of $\mathbf{TTF}^{+\bullet}CB^-$ at 295 K; in parenthesis are values measured in solutions of $\mathbf{TTF}^{+\bullet}ClO_4^-$. [e] From ref 21.

3.2. Dynamic Effects in the ESR Observation of $\mathbf{TTF}^{+\bullet}$ in Cross-Association. Further support for the facile cross-association (eq 3) of the cationic $\mathbf{TTF}^{+\bullet}$ attendant upon the incremental addition of the neutral **TTF** donor was indicated by the accompanying change in the ESR spectrum—initially observed as the broadening of each quintet line at the slow-

(33) (a) Jung, Y.; Head-Gordon, M. *Phys. Chem. Chem. Phys.* **2004**, *6*, 2008. (b) Note that direct comparison in the less polar dichloromethane was not possible, owing to the low solubility of the perchlorate salt. (c) Note that $\mathbf{TTF}^{+\bullet}CB^-$ crystallizes as the monomeric salt from various solvents at both room and low temperatures.[29f] Its solid-state absorption spectrum is similar to that characteristic of the monomeric $\mathbf{TTF}^{+\bullet}$ in solutions (see Figure S12).

(34) (a) Badger, B.; Brocklehurst, B. *Nature* **1968**, *219*, 263. (b) Badger, B.; Brocklehurst, B. *Trans. Faraday Soc.* **1969**, *65*, 2582; **1970**, *66*, 2939.

(35) Small, D.; Zaitsev, V.; Jung, Y.; Rosokha, S. V.; Head-Gordon, M.; Kochi, J. K. *J. Am. Chem. Soc.* **2005**, *127*, 7411.

exchange limit, followed by their gradual coalescence, and finally as the sharpened signal at the fast-exchange limit[36] (see Figure S10). Furthermore, the reversible character of such a dynamic line-broadening effect according to eq 3 was observed as an equivalent narrowing of the ESR lines as the temperature was lowered. [However, even at the lowest temperatures of 100 °C, we were unable to observe the doubling into the expected decet that is directly diagnostic of the dimeric cation-radical.[18,37]]

It must be mentioned that the diagnostic hyperfine line broadenings of organic ion-radicals in the presence of their diamagnetic parent have been extensively utilized in the quantitative evaluation of electron-transfer self-exchange rates between these species.[21,36]As such, the changes in the ESR line widths of $\mathbf{TTF}^{+\bullet}$ cation-radical measured (in different solvents in the slow-exchange limit) in the presence of various concentrations of neutral tetrathiafulvalene allowed us to evaluate the phenomenological (second-order) rate constants listed in Table 2 for the $\mathbf{TTF}^{+\bullet}/\mathbf{TTF}$ self-exchange according to eq 6:

$$\mathbf{TTF}^{+\bullet} + \mathbf{TTF} \overset{k_{SE}}{\rightleftharpoons} \mathbf{TTF} + \mathbf{TTF}^{+\bullet} \qquad (6)$$

Notably, the values of the second-order rate constant (k_{SE}) determined in solutions of the cation-radical with carborane counteranion ($\mathbf{TTF}^{+\bullet}CB^-$) in this work are close to those measured earlier[21] with the perchlorate salt ($\mathbf{TTF}^{+\bullet}ClO_4^-$). Furthermore, the temperature variations led to relatively small changes in the self-exchange rates, and the (linear) dependence of ln k_{SE}^{exp} with inverse temperature resulted in activation barriers for the $\mathbf{TTF}^{+\cdot}/\mathbf{TTF}$ self-exchange of E_a = 0.9 kcal mol^{-1} in dichloromethane and 1.4 kcal mol^{-1} in acetonitrile.

Discussion

The successful preparation of the unusual salt of tetrathiafulvalene cation-radical with the large, non-coordinating dodecamethylcarboranate counteranion offers us the unique opportunity to scrutinize its dimeric cation-radical as the first (dyad) member of π-stacked **TTF** arrays (with $n = 2$), i.e.,

Chart 1

$$(\mathbf{TTF})_2^{+\cdot} \overset{\pm e}{\Longleftrightarrow} \pi(\mathbf{TTF})_n$$

1. Distinctive Intermolecular Structures of Tetrathiafulvalene Associates. Exhaustive comparison of the various crystallographic structures of p-doped arrays extant in the X-ray literature,[22] together with the unambiguous structure of the dimeric dication,[22a,37] provides compelling evidence that all tetrathiafulvalene associates have the same basic (cofacial) structure, consisting of two **TTF** moieties either lying directly atop each other (A) or somewhat shifted laterally (B) at the relatively wide interplanar separation of $r_\pi = 3.5 \pm 2$ Å, as illustrated in Chart 2.[39]

Such a long-bonded dimeric structure with face-to-face **TTF** moieties is observed in the dicationic perchlorate salt consisting of two equivalent tetrathiafulvalene cation-radicals, [$\mathbf{TTF}^+$,$\mathbf{TTF}^+$].[22a]

Chart 2

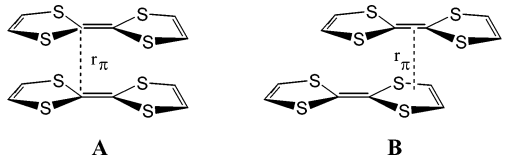

A **B**

Furthermore, essentially the same basic structure is also characteristic of monocationic dyads consisting of (a) two equivalent tetrathiafulvalene moieties with each bearing half a charge, [$\mathbf{TTF}^{0.5+}$,$\mathbf{TTF}^{0.5+}$], and (b) two inequivalent tetrathiafulvalene moieties with one cation-radical and the other neutral, [$\mathbf{TTF}^{+\bullet}$,**TTF**], as in the hexachlorostannate and tetrafluoroborate salts,[22b,c] respectively. Moreover, a similar cofacial arrangement (atop each other or slightly shifted laterally) has been identified as the basic structural unit present in p-doped (multicenter) arrays consisting of (a) a finite number of constituents for $(\mathbf{TTF})_n^{m+}$, where $2 < n < 9$, as in the tetrachloroferrate[22d] and tetracyanoplatinate[22e] salts, and (b) a large, indefinite number of constituents, as in the thiocyanate,[22f] nitrate,[22g] and tetracyanoquinodimethane (TCNQ) salts.[23]

From a different experimental perspective, the electronic spectrum of the distinctive (solid-state) dyad as the dicationic $(\mathbf{TTF})_2^{2+}$ unit is essentially the same as that of the $(\mathbf{TTF})_2^{2+}$ dication present in different solutions (being essentially invariant with different counterions and with changes in solvent polarity).[40a] Such a concordance of the electronic transitions indicates that the dyad structures are largely unaffected by the environment. In other words, structural and spectral data are consistent with dyad structures, which are determined principally by the overwhelming balance of attractive/repulsive forces[40b] between tetrathiafulvalene moieties—more or less independent of external perturbations and whether they bear either a +1 or +2 charge. As such, the resulting equilibrium structures of the monocationic and dicationic dyads in Chart 2 are minimally affected by either crystal forces or solvation (and independent of the nature of counteranion), to the degree that the interplanar separation of $r_\pi \approx 3.5$ Å persists in solution as in the solid state.

2. Electronic Structures of Mixed-Valence (Tetrathiafulvalene) Dyads. Central to the intermolecular electronic movement between juxtaposed **TTF** moieties in the mixed-valence dyad are the magnitude of the electronic coupling element (H_{ab}) and the intrinsic barrier given as the Marcus reorganization energy (λ). According to Hush, these parameters can be evaluated from the diagnostic (intervalence) optical transition in the mixed-valence [$\mathbf{TTF}^{+\bullet}$,**TTF**] complex in Figure 4, provided it is first assigned within the Robin−Day framework.[41] In order to establish whether the [$\mathbf{TTF}^{+\bullet}$,**TTF**] dyad belongs to Class II (localized) or Class III (delocalized), we first probe

(36) Chang, R. *J. Chem. Educ.* **1970**, *47*, 563.
(37) (a) Lewis, I. C.; Singer, I. C. *Chem. Phys* **1965**, *43*, 2712. (b) Howarth, O. W.; Fraenkel, G. K. *J. Am. Chem. Soc.* **1966**, *88*, 4514. (c) Lau, W.; Kochi, J. K. *J. Org. Chem.* **1986**, *51*, 1801.
(38) Scott, B. A.; LaPlaca, S. J.; Torrance, J. B.; Silverman, B. D.; Welber, B. *J. Am. Chem. Soc.* **1977**, *99*, 6631.
(39) (a) Consideration of the 70-odd stacked **TTF** structures extant in the Cambridge Crystallographic Database indicates a consistent but rather narrow variation in the interplanar separation of $r_\pi = 3.5 \pm 0.2$ Å. (b) However, the stacking structures fall essentially into two general classes, viz., the vertical and slipped dyads exemplified by structures A and B, respectively, in Chart 2. Furthermore, B stacks show variable displacements from the vertical of up to 1.5−2.0 Å. (c) The crossed **TTF** dyad at the same interplanar separation represents the rather unique exception. See: Triki, S.; Ouahab, L.; Halet, J. F.; Pena, O.; Padiou, J.; Grandjean, D.; Garrigou-Lagrange, C.; Delhaes, P. *J. Chem. Soc., Dalton Trans.* **1992**, 1217.
(40) (a) Note, however, the labile nature of the dimer in solution, as discussed in section 3.3. (b) For ab initio computations of the unique bonding extant in long-bonded π-dimers, see refs 17b, 33a, and 35.
(41) Robin, M. B.; Day, P. *Adv. Inorg. Chem. Radiochem.* **1967**, *10*, 247.

the solvent dependence of the intervalence (NIR) band, since the transition energy (ν_{IV}) is directly related to the donor/acceptor coupling (H_{ab}) in delocalized (Class III) complexes and largely unaffected by solvent polarity.[8,42] On the other hand, the transition energy in localized (Class II) complexes is related to the reorganization energy, consisting of separate inner-sphere (λ_i) and solvent (λ_s) components.[7,8] Since λ_s is determined as a product of factors related to the geometry of the redox system and to the static (ϵ_s) and optical ($\epsilon_o = n^2$) dielectric constants of solvent, the increase of the solvent polarity is generally accompanied by a significant blue-shift of the intervalence transition in Class II complexes.[8,43] We conclude from the substantial variation of the energy of the diagnostic NIR band in Table 2 (showing blue shifts in more polar solvents) that the [**TTF**$^{+\bullet}$,**TTF**] complex is localized in nature. Moreover, this assignment to Class II is supported by the clear correlation of the solvent dependence of the intervalence transition in this dyad—as also observed with analogous Class II systems, such as the mixed-valence complex of tetracyanoethylene anion-radical with its parent,[17b] or in bridged cation-radicals[43b] (see Figure S11 in the Supporting Information). This conclusion is also confirmed by the consistency of the values of reorganization energy derived from the optical transition with those resulting from ab initio computations (vide infra).

According to Mulliken−Hush theory,[12,13] the energy of the diagnostic NIR band in the Class II mixed-valence [**TTF**$^{+\bullet}$,**TTF**] complex provides the direct measure of the reorganization energy for electron transfer as $\lambda = \nu_{IV}$; these values are listed in Table 3 for solvents of different polarity. Furthermore, the integral intensity of the intervalence band (see Table S1 for spectral details), together with the separation parameter evaluated as $r_\pi = 3.5$ Å (vide supra), provides the experimental data for the application of Mulliken−Hush eq 1, and the values of H_{ab} for the mixed-valence [**TTF**$^{+\bullet}$,**TTF**] dyad measured in various solvents are presented in Table 3, column 3. The results in Table 3 indicate that the electronic coupling in the [**TTF**$^{+\bullet}$,**TTF**] dyad is singularly invariant with solvent polarity. Most importantly, the magnitude of H_{ab}, being less than half the reorganization energies, confirms the assessment of this π-complex as a localized (Class II) donor/acceptor dyad (vide supra).[8]

Table 3. Reorganization Energies, Coupling Element, and Free-Energy Barrier for Electron Transfer within [**TTF**$^{+\bullet}$,**TTF**] Dyads

solvent	λ,[a] $\times 10^3$ cm^{-1}	H_{ab},[b] $\times 10^3$ cm^{-1}	ΔG^*, kcal/mol
CH_2Cl_2	4.73	1.6	0.4
MeOH	5.46	1.4	0.8
acetone	5.71	1.4	1.0
DMF	5.92	1.6	1.0
CH_3CN	5.81	1.5	1.0
THF	5.13	1.5	0.7

[a] From $\lambda = \nu_{IV}$, where ν_{IV} is the energy of the NIR band maximum (λ_{IV} in Table 2). [b] Calculated via eq 1 with accuracy of $\pm 0.3 \times 10^3$ cm^{-1} (see Table S3 for details).

Although the electronic coupling within the mixed-valence [**TTF**,**TTF**]$^{+\bullet}$ dyad is relatively strong, it is insufficient to overwhelm the reorganization penalty, and the activation barrier for the first-order electron transfer is thus limited by[8]

$$\Delta G^* = (\lambda - 2H_{ab})^2/4\lambda \quad (7)$$

It is noteworthy that the values of ΔG^* in Table 3 all lie in the range from 0.4 to 1.0 kcal mol^{-1}, notably lower than $\Delta G^* = \lambda/4$, or roughly 4 kcal mol^{-1}.

3. Applicability of the Experimental (Electron-Transfer) Parameters, H_{ab} and λ. It is now opportune to examine the direct experimental (spectral) evaluation of the electron-transfer parameters, H_{ab} and λ (Table 3), in the light of the three independent perspectives of the [**TTF**,**TTF**]$^{+\bullet}$ complex relating to (a) intermolecular (electron-transfer) kinetics of **TTF**$^{+\bullet}$/**TTF** self-exchange, (b) theoretical computation of the reorganization energy, and (c) ab initio molecular-orbital evaluation of the solid-state coupling element, as follows.

3.1. [TTF,TTF]$^{+\bullet}$ as the Precursor Complex in Self-Exchange Kinetics. As the primary (diffusive) associate, [**TTF**$^{+\bullet}$,**TTF**] represents the precursor complex in the electron-transfer mechanism for self-exchange according to eq 2, where **D** = tetrathiafulvalene. As such, the overall rate of the self-exchange process is dependent on the equilibrium constant (K_{CT}) for the formation of the precursor (mixed-valence) complex and the intramolecular rate constant (k_{ET}), given as[8]

$$k_{ET} = A \exp(-\Delta G^*/RT) \quad (8)$$

The values of the rate constant k_{ET} for the [**TTF**$^{+\bullet}$,**TTF**] dyad calculated via eq 8 (using the reorganization barriers evaluated in the previous section and the pre-exponential factor of 10^{12} s^{-1})[16] are listed in Table 4, second column. Notably, the $k_{ET}K_{CT}$ product (with the formation constant of the precursor complex from Table 2) is faster than the bimolecular diffusion rates, as evaluated by k_{diff} listed in the third column of Table 4. Therefore, the self-exchange rate constant must be recalculated on the basis of

$$1/k_{SE}{}^{calc} = 2/k_{diff} + 1/K_{CT}k_{ET} \quad (9)$$

from the standard steady-state approximation,[44] and these values of the second-order rate constant for the **TTF**$^{+\bullet}$/**TTF** self-exchange in several solvents are listed in Table 4, column 4.

It is important to note that the calculated rate constants for self-exchange ($k_{SE}{}^{calc}$), based on the mechanism in eq 2, all correctly lie within half an order of magnitude of the experimental values of the second-order rate constant ($k_{SE}{}^{exp}$) listed in column 5 of Table 4. The calculated barrier for intracomplex

Table 4. Rate Constant for the **TTF**$^{+\bullet}$/**TTF** Self-Exchange

solvent	k_{ET}, $\times 10^{11}$ s^{-1}	k_{diff},[b] $\times 10^9$ M^{-1} s^{-1}	$k_{SE}{}^{calc}$, $\times 10^9$ M^{-1} s^{-1}	$k_{SE}{}^{exp}$,[a] $\times 10^9$ M^{-1} s^{-1}
CH_2Cl_2	5.4	15.1	7.5	2.7
CH_3CN	1.9	19	8.9	3.3
acetone	1.7	20.2	9.2	3.5
THF	3.4	11.4	5.5	2.3

[a] Measured in solution of **TTF**$^{+\bullet}$CB$^-$ at 295 K. [b] From ref 21.

(42) (a) Demadis, K. D.; Hartshorn, C. M.; Meyer, T. J. *Chem. Rev.* **2001**, *101*, 2655. (b) D'Alessandro, D. M.; Topley, A. C.; Davies, M. S.; Keene, R. F. *Chem. Eur. J.* **2006**, *12*, 4873.

(43) (a) As noted recently,[43b] the solvent dependence of the intervalence band for Class II systems can be presented as a linear combination of the Pekar factor for the solvent ($\gamma = 1/n^2 - 1/\epsilon_s$) and the Guttman donor number. (b) Nelsen, S. F.; Trieber, D. A., II; Ismagilov, R. F.; Teki, Y. *J. Am. Chem. Soc.* **2001**, *123*, 5684.

(44) Newton, M.; Sutin, N. *Annu. Rev. Phys. Chem.* **1986**, *35*, 435.

electron transfer, lying in the range of 0.5−1 kcal/mol, accords with the experimental activation energies for the self-exchange of about 1 kcal/mol (vide supra) that are determined from the temperature dependence of the ESR line-broadening. Such an accord of the calculated and experimental kinetics supports the Mulliken−Hush evaluation of the parameters governing thermal electron transfer.[45] Furthermore, the low barriers and high (intracomplex) ET rate constants imply that the intermolecular self-exchange process is mainly controlled by the solvent (diffusion) dynamics, and these values are rather insensitive to changes in the electron-transfer barrier (in the range of 0.5−1 kcal/mol).[46]

In order to further establish the validity of the electron-transfer parameters evaluated from the spectral data, let us now compare them with the results of ab initio computations as well as solid-state analysis.

3.2. Computational Evaluations of the Reorganization Energy. The intramolecular contribution (λ_i) to the overall reorganization energy within the [**TTF**$^{+\bullet}$,**TTF**] dyad is calculated as the difference between the initial diabatic state, with the electron located on the donor (**TTF**) and reactants in their relaxed geometries, and the final diabatic state, with the same nuclear geometry but the electron transferred to the acceptor (**TTF**$^{+\bullet}$):[17,47]

$$\lambda_i^{calc} = \{E_c(r_n) + E_n(r_c)\} - \{E_n(r_n) + E_c(r_c)\} \qquad (10)$$

where r_n and r_c are the optimized coordinates and E_n and E_c are the energies of the neutral donor and its cationic counterpart. Accordingly, we first optimize the geometry of the neutral and cationic tetrathiafulvalene and determine their energies, $E_n(r_n)$ and $E_c(r_c)$, via DFT computations with the aid of Gaussian 98 (6-311G* basis and B3LYP functional).[48] The single-point calculation of **TTF**$^{+\bullet}$ in the geometry of the neutral **TTF** then leads to $E_c(r_n)$, and the neutral donor in the geometry of the cation produces $E_n(r_c)$. The energy difference corresponds to $\lambda_i^{calc} = 2.3 \times 10^3$ cm^{-1}, or 6.8 kcal/mol (see Table S4 for details).

In order to calculate the solvent reorganization energy, the precursor complex is considered as a cavity with an internal dielectric constant of $\epsilon_{in} = 2$, immersed in a solvent with static and optical dielectric constants ϵ_s and ϵ_o.[17,49] The reorganization energy, λ_o^{calc}, based on the Kirkwood solvation model is given by[49]

$$\lambda_o^{calc} = 1/2a_0\{(1/\epsilon_{in} - 1/\epsilon_s)\sum_n g_n/(1 + [n/(n+1)]\epsilon_{in}/\epsilon_s) - (1/\epsilon_{in} - 1/\epsilon_0)\sum_n g_n/(1 + [n/(n+1)]\epsilon_{in}/\epsilon_0)\} \qquad (11)$$

where $g_n = \Sigma\Sigma\Delta e_k \Delta e_j (r_k/a_0)^n (r_j/a_0)^n P_n(\cos\theta_{jk})$, with $n = 1-6$, Δe_j denotes the variation of the charge on the jth atom, N is the number of atoms, r_j locates the jth atom in space, θ_{jk} is the angle between r_j and r_k, and P_n are ordinary Legendre functions. The atomic coordinates in the precursor complex are taken from the X-ray structures of the related (**TTF**)$_2^{2+}$ diamagnetic dimer,[22a] and the value of $a_0 = 4.85$ Å is calculated from the molecular volume of 207.5 cm^3 M^{-1} (obtained by single-point Gaussian 98 computation of this dyad) plus 0.5 Å.[17,48] The atomic charges of the cationic and neutral **TTF** donor constituting the complex in the hypothetical diabatic state are taken via the Gaussian 98 computation of the isolated species (ESP charges, CHELPG option[48]). The values of the reorganization energies calculated in this way in several solvents are listed as λ_o^{calc} in column 2 of Table 5. To account for the labile nature of the precursor complex (such that the optical and thermal electron transfer can occur at various donor/acceptor orientations), the solvent reorganizations are also calculated for different isomeric forms of the precursor complex, produced by an artificial variation of the interplanar separation from 3.3 to 4.0 Å and consisting of both laterally shifted and crossed **TTF** moieties.[50] Significantly, the values of λ_o calculated for different configurations are all within 20% of that calculated for the prototypical structure listed in Table 5.

Table 5. Computed Reorganization Energies for the Mixed-Valence (**TTF**)$_2^{+\bullet}$ Complex in Various Solvents

solvent	λ_o^{calc}, $\times 10^3$ cm^{-1}	λ^{calc}, $\times 10^3$ cm^{-1}	λ^a, $\times 10^3$ cm^{-1}
CH_2Cl_2	2.1	4.4	4.7
MeOH	3.0	5.3	5.5
acetone	2.8	5.1	5.7
DMF	2.7	5.0	5.9
CH_3CN	2.9	5.2	5.8
THF	2.0	4.3	5.1

[a] Determined as $\lambda = \nu_{IV}$.

The sum of the outer-sphere and inner-sphere components (taken as constant at 2.3×10^3 cm^{-1}) leads to the total reorganization energies for the (**TTF**$^{+\bullet}$,**TTF**) dyad listed as λ^{calc} in column 3 of Table 5. It is thus noteworthy that the comparisons in Table 5 indicate that reasonable agreement is achieved between the calculated values (λ^{calc}) and the experimental reorganization energies (λ) derived from the Mulliken−Hush treatment of the intervalence spectrum.

3.3. Ab Initio Computations and Solid-State Evaluations of the Coupling Element. The ab initio evaluation of the electronic coupling element between equivalent donor/acceptor moieties within the dimeric species is based on the energy splitting resulting from symmetric and antisymmetric combinations of the localized nth molecular orbitals of the corresponding monomers, i.e.,[9−11]

$$H_{ab} = {}^1/_2\,[E_{n,1} - E_{n,2}] \qquad (12)$$

In the cationic mixed-valence dimer, the coupling element is

(45) By way of contrast, the classical Marcus evaluation of the (second-order) self-exchange rate constant, given as[8] $k_{SE} = 10^{11}\exp(-\lambda/4RT)$, predicts significantly lower values of 0.3×10^9 M^{-1} s^{-1} in dichloromethane, 0.07×10^9 M^{-1} s^{-1} in acetonitrile, 0.08×10^9 M^{-1} s^{-1} in acetone, and 0.2×10^9 M^{-1} s^{-1} in tetrahydrofuran solutions.

(46) As such, the experimental barrier E_a represents a composite of the electron-transfer barrier, the thermodynamics of the precursor complex, and the temperature dependence of the diffusion rate constant.

(47) (a) Nelsen, S. F.; Blackstock, S. C.; Kim, Y. *J. Am. Chem. Soc.* **1987**, *109*, 677. (b) Perng, B.-C.; Newton, M. D.; Raineri, F. O.; Friedman, H. L. *J. Chem. Phys.* **1996**, *104*, 7153. (c) Blomgren, F.; Larsson, S.; Nelsen, S. F. *J. Comput. Chem.* **2001**, *22*, 655.

(48) Pople, J. A.; et al. *Gaussian 98*, Revision A.11.3; Gaussian, Inc.: Pittsburgh, PA, 1998.

(49) Vener, M. V.; Ioffe, N. T.; Cheprakov, A. V.; Mairanovsky, V. G. *J. Electroanal. Chem.* **1994**, *370*, 33.

(50) For example, calculations of outer-sphere reorganization energies for [**TTF**$^{+\bullet}$,**TTF**] in dichloromethane led to the values of $\lambda_o = 2.0 \times 10^3$, 2.3×10^3, and 2.5×10^3 cm^{-1} for the face-to-face complex in Chart 1 at interplanar separations of 3.3, 3.7, and 4.0 Å, respectively, and $\lambda_o = 2.2 \times 10^3$ cm^{-1} for the dyad with the interplanar separation of 3.5 Å and the lateral shift of 1.5 Å.

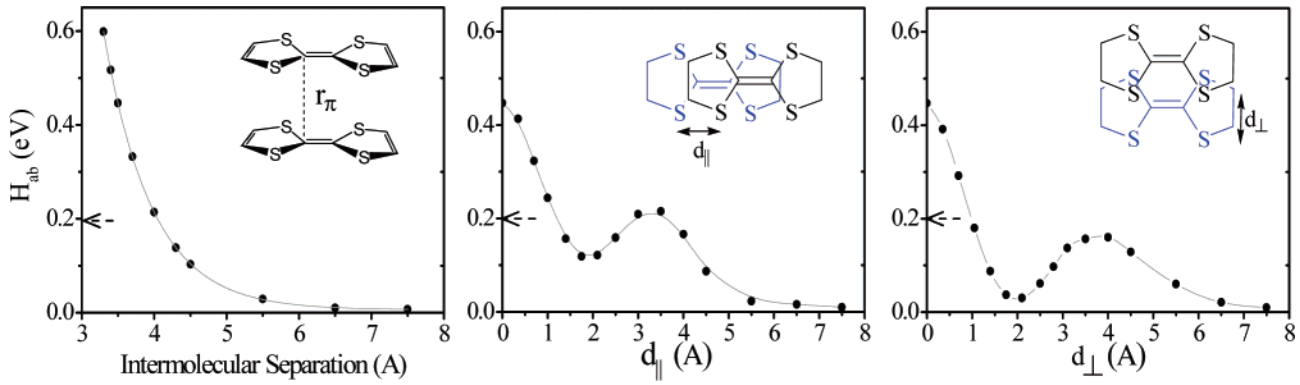

Figure 5. Electronic coupling element calculated from the HOMO splitting (eq 12) for various geometries of tetrathiafulvalene π-dimers (arrows indicate Mulliken−Hush value, for comparison).

calculated from the pairwise splitting of the HOMO orbital of the parent donor.[11] According to Huang and Kertesz,[10] the electronic coupling obtained at different levels of theory for the tetrathiafulvalene dimeric unit lies in the range from 0.14 to 0.21 eV (at 295 K). It is thus noteworthy that the electronic coupling of $H_{ab} \approx 0.19$ eV, evaluated here from the intervalence absorption spectrum, lies in the midrange of the ab initio results. Most importantly, the solid-state ESR, ^{13}C NMR, plasma frequency, and thermoelectric power studies are all in accord with the value of $V = 0.12 \pm 30\%$ eV for the transfer integral between tetrathiafulvalene moieties along their stacks in [**TTF**,**TCNQ**] crystals.[23] As such, both ab initio and Mulliken−Hush (spectral) values of the coupling elements for pairwise interaction within the tetrathiafulvalene dyad agree reasonably well with the experimental estimates deduced from solid-state properties involving cooperative interactions within (essentially) infinite stacks.

It must be mentioned, however, that in the [**TTF**,**TCNQ**] salt, the donor and acceptor entities form infinite segregated stacks in which tetrathiafulvalene moieties lie parallel at the interplanar separation of $r_\pi \approx 3.45$ Å and shifted laterally along the main axis by about 1.5 Å. Such a shift generally results in a decrease of the electronic coupling due to the longitudinal offset.[5,10] Additionally, the center-to-center separation of 3.8 Å is somewhat wider than our value for the calculation of H_{ab} via the Mulliken−Hush eq 1.

To establish the structural dependence of the coupling element in more detail, we extended the Huang−Kertesz analysis[10] and carried out the (in vacuo) computations of the HOMO splitting resulting from their symmetric and antisymmetric combinations within the corresponding **TTF** dimers (B3LYP calculations with 6-31G* basis set[48]). [The shapes of the corresponding orbitals are illustrated in Chart S1 in the Supporting Information.] The dimer geometry (see Table S5 in the Supporting Information) was taken from the X-ray structure of $[\mathbf{TTF}_2]^{2+}(ClO_4^-)_2$,[22a] in which two tetrathiafulvalene moieties are arranged atop each other, as in Chart 2A. This arrangement was then modified by varying the separation (r_π) or by shifting one of tetrathiafulvalene moieties either parallel ($d_{||}$) or perpendicular ($d_\perp$) to the central C−C bonds at a constant value of $r_\pi = 3.5$ Å. In contrast to the reorganization energy,[50] these computations show a considerable dependence of the electronic coupling element on the structure of the precursor complex, as illustrated in Figure 5. In other words, the increasing intermolecular separation is accompanied by the exponential decay of the coupling element, so that $H_{ab} = 0.45$ eV (3600 cm^{-1}) at the standard separation of $r_\pi = 3.5$ Å. The longitudinal and perpendicular offsets (at the same separation of $r_\pi = 3.5$ Å) also lead to dramatic decreases of the computed coupling elements.[51] Furthermore, the mutual rotation of the tetrathiafulvalene moieties also decreases the coupling elements, so that the perpendicularly crossed structure[39c] separated by $r_\pi = 3.5$ Å is characterized by $H_{ab} = 0.35$ eV (2800 cm^{-1}).

Notably, the (in vacuo) computation of the coupling element for the vertical dimer illustrated in Chart 2A leads to the value of $H_{ab} = 3600$ cm^{-1} ($r_\pi = 3.5$ Å), which is more than twice the experimental values of 1500−1600 cm^{-1}, based on Mulliken−Hush (spectral) analysis. In order to reconcile these results, we recognize that the **TTF** dyad is rather unusual in two important ways. First, such long-bonded dimers are characterized by a rather broad, shallow potential energy minimum,[17b,33a,35,52] and second, the complex shape of the HOMO points to the existence of several local-energy minima.[51] As such, various mutual arrangements of **TTF** moieties with comparable energies are likely to coexist *in solution*. Accordingly, the (Mulliken−Hush) spectral estimation of H_{ab} represents the integral averaged value, and any rigorous comparison would require evaluation of the energetics and relative contributions of the various molecular arrangements. Taking into account that any deviation from the geometry in Chart 2A results in dramatic decreases of H_{ab} (Figure 5), the averaging of the (ab initio) values of H_{ab}, representing a variety of conformations (librations) around this basic structure (derived by lateral shifts and/or rotation of one **TTF** moieties in the plane) in solution, will lead to a value which agrees reasonably with the Mulliken−Hush estimation.

The mutual consistency among the ab initio computations, the Mulliken−Hush analysis, and the solid-state estimates of the coupling element thus confirms the validity of all these methodologies and supports the similarity of the pairwise intermolecular interactions in isolated dyads in solutions with those occurring in indefinite solid-state stacks. Furthermore, the

(51) However, the curves in Figure 5B,C (H_{ab} vs $d_{||}$ or $d_\perp$) show additional local maxima, similar to those reported for some other long-bonded π-dyads.[4,10] Such dependences result from the complex nodal shape of the tetrathiafulvalene HOMO (see Chart S1 in the Supporting Information), since its symmetry simultaneously favors bonding interaction for (i) the vertical structure A, (ii) certain relative (parallel or perpendicular) displacements B in Chart 2, and, in addition, (iii) the perpendicularly crossed structure,[39c] such that structural changes occurring *within the **TTF** plane* are (more or less) equally accessible. This orbital (symmetry) situation differs from that of some other systems, such as TCNE/TCNE$^{-\bullet}$ (see refs 10, 17, and 33a).

(52) Novoa, J. J.; Lafuente, P.; Del Sesto, R. E.; Miller, J. S. *Angew. Chem., Int. Ed.* **2001**, *40*, 2540.

magnitude of the electronic coupling element (H_{ab}) relative to the intrinsic barrier, given as the reorganization energy, λ, is central to the intermolecular electronic movement between juxtaposed **TTF** moieties. Our measurements of $H_{ab} = 1.6 \times 10^3$ cm^{-1} and $\lambda = 4.8 \times 10^3$ cm^{-1} in Table 3 thus indicate that the effective barrier for the electron transfer between the two faces of (**TTF**)$_2$ in dichloromethane solutions is 140 cm^{-1}, or $\Delta G_{ET}^* \approx 0.4$ kcal mol^{-1}. According to the conventional Robin−Day classification of mixed-valence complexes,[8,41] the relative energy of $2H_{ab}/\lambda = 0.68$ identifies a Class II system, in which the electron-transfer step occurs between a pair of equivalent ground states:

$$[\mathbf{TTF}^{+\bullet},\mathbf{TTF}] \overset{\Delta G_{ET}^*}{\rightleftharpoons} [\mathbf{TTF},\mathbf{TTF}^{+\bullet}] \qquad (13)$$

The trend in the solvent sensitivity of the reorganization energy in Table 3, column 2, predicts an increasing barrier for intracomplex electron transfer and a decreasing rate of electron transfer in a polar solvent environment. On the other hand, in the absence of solvation (in which the outer-sphere component in Table 5 is nil), our computation leads to the reorganization energy of $\lambda = 2.3 \times 10^3$ cm^{-1}. Coupled with the measured magnitude of $H_{ab} = 1.6 \times 10^3$ cm^{-1}, the ground state of (**TTF**)$_2^{+\bullet}$ in vacuo is predicted to consist of a single minimum, in which the odd electron is completely delocalized between both **TTF** moieties diagnostic of Class III complexes.

Although evaluation of the electronic movement within the mixed-valence (**TTF**)$_2^{+\bullet}$ dyad in vacuo is not applicable in toto to that in p-doped (multicenter) **TTF** arrays, the relative values of coupling element and inner-sphere reorganization energy imply that, if the outer-sphere component is less than 1×10^3 cm^{-1}, the mixed-valence system will be delocalized, but any further increase will induce localization. As such, minimal changes in environment can be responsible for transitions from Class III to Class II, and vice versa.

Summary and Conclusions

The unusual solubility of the tetrathiafulvalene cation-radical salt (**TTF**$^{+\bullet}$CB$^-$) with the non-coordinating (charge-delocalized) dodecamethylcarborane anion in a variety of organic solvents provides the opportunity to examine minimally disturbed intermolecular π-interactions of the **TTF**$^{+\bullet}$ of interest as related to its solid-state conductivity. Thus,**TTF**$^{+\bullet}$ shows a strong tendency to undergo π-dimerization, in which the long-distance attractive interaction overcomes the electrostatic repulsion, even in moderately polar environments. The long-bonded dimers[40,52] are characterized by strong absorptions in the visible region, showing two bands closely related to the local transitions in **TTF**$^{+\bullet}$ monomer (but with typical Davydov's blue-shift[24,32]) and a low-energy band at 730−755 nm arising from the $\pi-\pi$ interactions of the monomer SOMO. Importantly, the spectral properties of the dimer are essentially the same in all solvents, suggesting minimal disturbance of its structure by solvation. Moreover, its similarity to the solid-state absorption of the dimer implies a direct relationship of the X-ray-determined structure to that present in solution.

The bimolecular interaction of the **TTF**$^{+\bullet}$ cation-radical with the parent **TTF** results in the formation of the mixed-valence π-dimer [**TTF**$^{+\bullet}$,**TTF**], which shows an intense solvent-dependent intervalence absorption band in the NIR range, in addition to the unaffected local (UV−vis) bands of the **TTF**$^{+\bullet}$ cation-radical. Significant solvent dependence of the intervalence band allows the assignment of this mixed-valence complex to Robin−Day Class II. Mulliken−Hush analysis of the NIR absorption (together with structural data on tetrathiafulvalene associates) provides the experimental basis for the evaluation of the electronic parameters governing thermal electron transfer within the tetrathiafulvalene dyad. As such, the reorganization energy evaluated from the spectral data ranges from $\lambda = 4.7 \times 10^3$ cm^{-1} in dichloromethane to 6.3×10^3 cm^{-1} in DMF, in accord with the theoretical (quantum-mechanical) computations of the inner-sphere λ_i of 2.3×10^3 cm^{-1} and the solvent-dependent λ_o of $(2.4-3.5) \times 10^3$ cm^{-1}. Spectral and structural analyses of the mixed-valence dyad based on Mulliken−Hush theory leads to the coupling element $H_{ab} = 1.5 \times 10^3$ cm^{-1}. Such a significant coupling energy points to the free-energy barrier of only 0.5−1.0 kcal M^{-1} for electron transfer within the tetrathiafulvalene dyad, in agreement with the experimental second-order self-exchange kinetics. The Mulliken−Hush evaluation of H_{ab} is also consistent with recent ab initio computations and the experimental solid-state estimate of the transfer integral. The latter thus supports the validity of different approaches (involving pairwise interactions) to evaluate the electronic interactions within infinite stacks that are essential for the solid-state determination of the coupling element.

Experimental Section

Tetrathiafulvalene (Acros) was purified by sublimation in vacuo, and the **TTF**$^{+\bullet}$CB$^-$ salt was produced by the oxidation of **TTF** with an equimolar amount of dodecamethylcarboranyl[27,28] in CH_2Cl_2, followed by precipitation with hexane. Solvents were prepared and handled as described earlier.[16]

The thermodynamics of dimerization and the extinction coefficient of the [**TTF**$_2$]$^{2+}$ dimer were determined as follows. The expressions for the equilibrium constant, $K_D = c_D/c_M^2$ (where c_D and c_M are the equilibrium concentrations of dimer and monomer, respectively), and the material balance, $2c_D + c_M = c_0$, lead to the overall relationship $4K_Dc_D - c_D(4Kc_0 + 1) + Kc_0^2 = 0$. The solution of this quadratic equation results in the expression of c_D in terms of K_D and c_0 as $c_D = \{(4K_Dc_0 + 1) - ((4K_Dc_0 + 1)^2 - 16K_D^2c_0^2)^{0.5}\}/8K_D = (4c_0 + 1/K_D)/8 - (8Kc_0 + 1)^{0.5}/8K_D$. On the other hand, the absorption of the **TTF**$^{+\bullet}$CB$^-$ solution in a 1-cm cuvette is expressed as $A = \epsilon_Dc_D + \epsilon_Mc_M$ (ϵ_D and ϵ_M are the extinction coefficients of the monomer and dimer, respectively, at a particular wavelength). As such, the absorption at the dimer band maximum (e.g., 755 nm in ethanol) is given by A(calc) $= \epsilon_Dc_D + \epsilon_M(c_0 - 2c_D)$, with $c_D = (4c_0 + 1/K_D)/8 - (8Kc_0 + 1)^{0.5}/8K_D$. Computer fitting (by the variation of K_D and ϵ_D) of A(calc) to the experimental absorption A(exp) (normalized to a 1-cm cuvette, if necessary) produces a unitary set of K_D and ϵ_D values which completely describe the absorption of the **TTF**$^{+\bullet}$CB$^-$ solution in the wide concentration range shown in Figure 6. (See also Figure S4 in the Supporting Information.)

It is important to emphasize that the thermodynamic and spectral characteristics determined from the room-temperature measurements coincide with the corresponding values determined independently from the temperature-dependent UV−vis and ESR measurements carried out in the manner described earlier,[32] and the single set of thermodynamic parameters accounts for all the UV−vis and ESR data over the entire 100 °C temperature span and concentrations ranging from 0.0007 to 0.01 M. The experimental procedures for the UV−vis−NIR measurements of the mixed-valence complex [**TTF**$^{+\bullet}$,**TTF**] were carried out as described earlier.[16] Self-exchange rates were evaluated in the slow-exchange limit by measuring the changes in the ESR line widths of

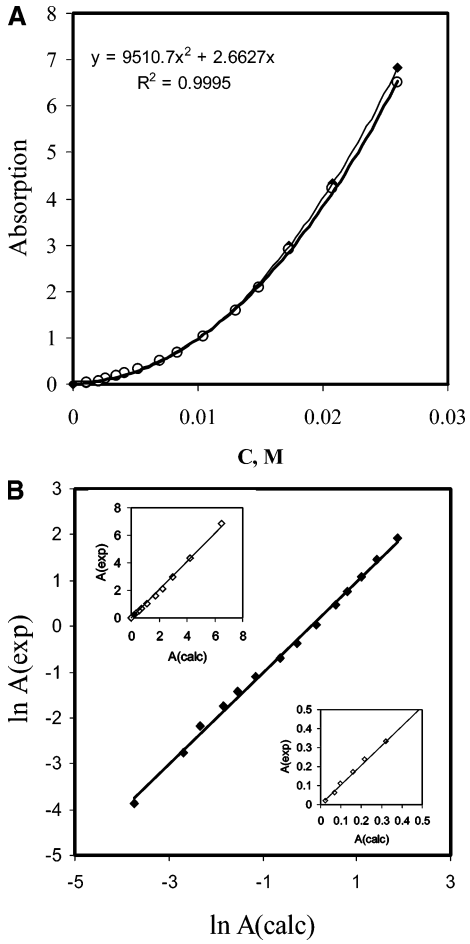

Figure 6. (A) Quadratic concentration dependence of the absorption at $\lambda_{max} = 752$ nm (at 22 °C) of **TTF**$^{+\bullet}$CB$^-$ dissolved in acetone (normalized to $\lambda = 1$ cm; rhombics, original data; circles, corrected for absorption of monomer). The equation presents the Excel-calculated second-order polynomial trend-line. (B) Relationship between the experimental absorption measured in acetone solutions of **TTF**$^{+\bullet}$CB$^-$ with concentrations from 1 to 26 mM at 22 °C (normalized to $\lambda = 1$ cm) and the values calculated as described in the text according to the dimerization equilibrium in eq 4, with $K_D = 0.42$ M^{-1}, $\epsilon_D(752) = 22\,500$ M^{-1} cm^{-1}, and $\epsilon_M(752) = 13$ M^{-1} cm^{-1}. (Note that the relationship is illustrated as the logarithmic function to cover the entire concentration range, and the insets represent the non-logarithmic data in the high- and low-concentration ranges.)

TTF$^{+\bullet}$ cation-radical in the presence of added **TTF** donor as also described previously.[17a]

Intensity data for X-ray crystallographic analysis were collected at −100 °C with a Brucker SMART Apex diffractometer using Mo Kα radiation ($\lambda = 0.71073$ Å). The structures were solved by direct methods and refined by full matrix least-squares treatment.[53] The structural details are on deposit and can be obtained from the Cambridge Crystallographic Database. Single crystals of **TTF**$^{+\bullet}$CB$^-$ were prepared by diffusion of hexane into the dichloromethane solution of the salt at −65 °C. **TTF**$^{+\bullet}$CB$^-$: formula, $C_{19}H_{40}B_{11}S_4$; M_w, 515.66; monoclinic, $P2(1)/n$; $a = 9.1393(8)$, $b = 13.3909$ (13), and $c = 12.5744(10)$ Å; $\beta = 109.609(5)°$; $V = 1449.6(2)$ Å^3; $D_c = 1.181$ g cm^{-3}; $Z = 2$. The total number of reflections measured was 13 301, of which 4128 were symmetrically nonequivalent. Final residuals were $R1 = 0.0454$ and w$R2 = 0.1292$ for 3505 reflections with $I > 2\sigma(I)$.

Acknowledgment. We thank J.-M. Lu for the preparation and spectral measurements of **TTF**$^{+\bullet}$ClO$_4^-$, T. Y. Rosokha for the preparation of **TTF**$^{+\bullet}$CB$^-$ single-crystals, S. M. Dibrov for X-ray crystallographic analysis of **TTF**$^{+\bullet}$CB$^-$, and the R. A. Welch Foundation and National Science Foundation for financial support.

Supporting Information Available: Dependence of the low-energy absorption on the concentration of **TTF**$^{+\bullet}$CB$^-$ in acetone (Figures S1, S2 and Table S1) and in ethanol (Figures S3, S4 and Table S2); temperature-dependent absorption of **TTF**$^{+\bullet}$CB$^-$ in ethanol (Figure S5); concentration dependence of the low-energy absorption of **TTF**$^{+\bullet}$CB$^-$ in acetonitrile and DMF (Figure S6); temperature-dependent **TTF**$^{+\bullet}$CB$^-$ absorption of **TTF**$^{+\bullet}$CB$^-$ in acetonitrile, DMF, dichloromethane, and THF (Figure S7); temperature-dependent NIR absorption spectra of dichloromethane solutions containing **TTF**$^{+\bullet}$CB$^-$ and **TTF** (Figure S8); NIR spectral changes showing the formation of the mixed-valence [**TTF**$^{+\bullet}$,**TTF**] complex in acetone, diethyl ether, acetonitrile, DMF, and THF (Figure S9); ESR spectra of **TTF**$^{+\bullet}$ cation-radicals in the presence **TTF** (Figure S10); correlations of the intervalence transition energies of the [**TTF**$^{+\bullet}$,**TTF**] dyad with those of [TCNE$^{-\bullet}$,TCNE] and bridged nitrogen-centered cation-radicals (Figure S11); solid-state spectrum of **TTF**$^{+\bullet}$CB$^-$ (Figure S12); details of the calculations of H_{ab} (Table S3) and λ_i (Table S4); molecular orbital shapes for the **TTF** HOMO and its splitting in the dimeric species (Chart S1); Cartesian coordinates of [**TTF**$^{+\bullet}$,**TTF**$^{+\bullet}$] dimer (Table S5); and complete ref 48; and X-ray crystallographic data, in CIF format, for **TTF**$^{+\bullet}$CB$^-$. This material is available free of charge via the Internet at http://pubs.acs.org.

JA064166X

(53) (a) Sheldrick, G. M. *SADABS*, Version 2.03; Bruker/Siemens Area Detector Absorption and Other Corrections, 2000. (b) Sheldrick, G. M. *SHELXS 97—Program for Crystal Structure Solutions*; University of Göttingen: Göttingen, Germany, 1997. (c) Sheldrick, G. M. *SHELXL 97—Program for Crystal Structure Refinement*; University of Göttingen: Göttingen, Germany, 1997.